J. Fluid Mech. (1981), *vol.* 105, *pp.* 239–260
Printed in Great Britain

Potential flow near conical stagnation points

By P. G. BAKKER, W. J. BANNINK

Department of Aerospace Engineering, University of Technology, Delft, The Netherlands

AND J. W. REYN

Department of Mathematics, University of Technology, Delft, The Netherlands

(Received 9 July 1979 and in revised form 27 June 1980)

Flow patterns near conical stagnation points in supersonic flow have been investigated on the basis of potential flow. Near the conical stagnation point the nonlinear equation for the conical velocity potential reduces to the equation of Laplace. Solutions of the equation of Laplace for incompressible plane flow are then used as a guide to generate conical stagnation-point solutions. Apart from known types of streamline patterns, such as nodes and saddle points, new types are found. Among them are oblique saddle points, saddle-nodes, topological nodes and topological saddle points. They may be used to clarify certain questions in a number of practical conical-flow problems. The oblique saddle point may be used to describe the inviscid flow associated with flow separation and also certain features of the flow over an external corner. The saddle-node, being structurally unstable, may fall apart into a saddle and a node. It may then be used to interpret the lift-off phenomenon of the singularity in the flow around a circular cone at incidence as a bifurcation. Similarly, this may be done for the appearance of a dividing streamline in the same flow at still higher angles of incidence, where a vortex system is formed at the leeward side of the cone.

1. Introduction

For three-dimensional flows of an inviscid, non-heat-conducting gas the notion of conical flow has been frequently used, in particular for supersonic flows past conically shaped bodies. In conical flow, the velocity and the conditions defining the state of the gas (pressure, density and temperature) are constant along rays emanating from a common point, the centre of the conical flow field. A conical flow may then be represented on a unit sphere around this centre. The velocity vector may be decomposed into a radial component and a component normal to the radius. From the latter a velocity vector field tangent to the unit sphere may be constructed. Integration of this vector field yields lines on the unit sphere which will be called conical streamlines. Points where the tangential velocity component vanishes will be called conical stagnation points. In conical flows with entropy gradients the entropy remains constant along conical streamlines. Then, if in a conical stagnation point various conical streamlines merge, an entropy singularity or vortical singularity is formed in such a point.

This idea was put forward by Ferri (1951) in relation to the supersonic flow past a circular cone at incidence for which he also introduced the concept of the vortical layer

near the cone surface. When using linearized theory to calculate the flow field, usually with the aim of obtaining pressure distributions on body surfaces, conical stagnation points are of secondary importance. If the full nonlinear flow equations are used, however, and numerical solution techniques become indispensable, a qualitative understanding of the flow field is necessary, and attention then focuses on the flow structure near conical stagnation points. It is of value, therefore, to evaluate as systematically as possible, by means of a local analysis, the possible flow structures near such points, so that in a particular flow problem the qualitative basis for a numerical procedure can be selected with more certainty. Since the appearance of Ferri's paper, investigations of the flow near conical stagnation points show an emphasis of interest in the possible conical streamline patterns, and related pressure distributions near such points. Melnik (1967) constructed some approximate solutions of the nonlinear inviscid conical flow equations in the neighbourhood of a conical stagnation point on a body surface. These solutions involve entropy gradients in the flow. When the streamline pattern was related to the corresponding pressure distribution on the body surface, no unique correspondence was found. Bakker (1977) showed that for these solutions a unique correspondence may be obtained if the pressure distribution normal to the body surface is also taken into account. Both papers indicate that the presence of entropy gradients does not affect the qualitative behaviour of the streamline pattern corresponding to a given pressure distribution. This result is further confirmed in the special case of the conical stagnation points in the flow past slender circular cones at high incidence, when calculated using slender body theory (Smith 1972), or linearized theory (Bakker & Bannink 1974).

In view of this, in the present paper a further study is made of conical stagnation points, using the assumption of potential flow. An advantage of this approach is that the nonlinear equations for conical flow reduce to a single second-order equation for the conical potential for which solutions are simpler to obtain. Moreover, in a conical stagnation point, this equation becomes the equation of Laplace, which is also satisfied by the velocity potential for an incompressible plane flow. Stagnation-point solutions for incompressible plane flows are then used as a guide to solutions near conical stagnation points. Also, a comparison of the two types of flows may be made by tracing systematically the influence of the existence of the radial velocity component in the case of conical flow. The analysis in the present paper reveals both known streamline patterns as well as new types. Particular flow problems are discussed to illustrate the use of the given classification.

2. Potential flow solutions near conical stagnation points

Consider an inviscid, non-heat-conducting perfect gas with ratio of specific heats $\gamma = c_p/c_v$. If the flow is irrotational, a velocity potential $\Phi = \Phi(x, y, z)$ may be introduced, such that $\nabla\Phi = \mathbf{q} = (u, v, w)$, where u, v and w are the components of the velocity $\mathbf{q}$ along the x, y and z axes in a right-handed Cartesian co-ordinate system, respectively. From the conservation of mass and momentum and the isentropic law it may be derived that Φ satisfies

$$(a^2-u^2)\,\Phi_{xx}+(a^2-v^2)\,\Phi_{yy}+(a^2-w^2)\,\Phi_{zz}-2uv\Phi_{xy}-2uw\Phi_{xz}-2vw\Phi_{yz}=0, \qquad (1)$$

where the speed of sound a is related to the velocity by

$$a^2 = \tfrac{1}{2}(\gamma-1)(q_{\max}^2 - u^2 - v^2 - w^2), \tag{2}$$

and $q_{\max}$ is the maximum speed, which we assume to be constant throughout the flow field. Equations (1) and (2) allow velocities to be non-dimensionalized by dividing them by $q_{\max}$; as a result we put $q_{\max} = 1$ in (2).

We will take the origin (0, 0, 0) in the centre of the conical flow field and the positive x axis along the ray corresponding to the conical stagnation point. Introducing in (1) the conical variables $\eta = y/x$ and $\zeta = z/x$ and the conical potential F defined by

$$\Phi = xF(\eta, \zeta), \tag{3}$$

yields

$$[a^2(1+\eta^2) - (v-u\eta)^2]F_{\eta\eta} + 2[a^2\eta\zeta - (v-u\eta)(w-u\zeta)]F_{\eta\zeta} + [a^2(1+\zeta^2) - (w-u\zeta)^2]F_{\zeta\zeta} = 0, \tag{4}$$

where

$$u = F - \eta F_\eta - \zeta F_\zeta, \quad v = F_\eta, \quad w = F_\zeta. \tag{5}$$

In the variables η and ζ the conical streamlines obey the equation

$$\frac{d\zeta}{d\eta} = \frac{w-u\zeta}{v-u\eta} = \frac{-\zeta F + \eta\zeta F_\eta + (1+\zeta^2)F_\zeta}{-\eta F + (1+\eta^2)F_\eta + \eta\zeta F_\zeta}. \tag{6}$$

It is sometimes convenient to work with polar co-ordinates $\eta = \rho\cos\phi$, $\zeta = \rho\sin\phi$, $-\infty < \phi < \infty, \rho \geqslant 0$; then the velocity components become

$$u = F - \rho F_\rho, \quad v = F_\rho\cos\phi - \frac{1}{\rho}F_\phi\sin\phi, \quad w = F_\rho\sin\phi + \frac{1}{\rho}F_\phi\cos\phi, \tag{7}$$

and (4) can be written as

$$a^2\left(F_{\rho\rho} + \frac{1}{\rho^2}F_{\phi\phi} + \frac{1}{\rho}F_\rho\right) + [a^2\rho^2 - \{\rho F - (1+\rho^2)F_\rho\}^2]F_{\rho\rho} + 2\left\{F - \left(\rho + \frac{1}{\rho}\right)F_\rho\right\}\left(\frac{1}{\rho}F_{\rho\phi} - \frac{1}{\rho^2}F_\phi\right)F_\phi - \left(\frac{1}{\rho^2}F_{\phi\phi} + \frac{1}{\rho}F_\rho\right)\frac{F_\phi^2}{\rho^2} = 0, \tag{8}$$

whereas the conical streamlines obey the equation

$$\frac{d\rho}{d\phi} = \frac{(1+\rho^2)\rho^2 F_\rho - \rho^3 F}{F_\phi}. \tag{9}$$

The direction of flow on a conical streamline may be obtained from

$$x\frac{d\eta}{dt} = v - u\eta, \quad x\frac{d\zeta}{dt} = w - u\zeta \tag{10}$$

or

$$x\frac{d\rho}{dt} = (1+\rho^2)F_\rho - \rho F, \quad x\frac{d\phi}{dt} = \frac{1}{\rho^2}F_\phi, \tag{11}$$

where t indicates time.

With the chosen co-ordinate system, the conical stagnation point is located in $\eta = \zeta = 0$ and, since $v = w = 0$ there, (4) yields

$$F_{\eta\eta}(0,0) + F_{\zeta\zeta}(0,0) = 0. \tag{12}$$

If the velocity components are assumed to be continuous in a neighbourhood of the

origin, (12) shows that (4) in this neighbourhood is approximately the equation of Laplace, which is also satisfied by the velocity potential Φ in incompressible plane flow. In polar co-ordinates, stagnation-point solutions for incompressible plane flow are given by

$$\Phi = a_n \rho^n \cos(n\phi + \psi_n), \quad n > 1, \tag{13}$$

where a_n, ψ_n are constants. They represent flows in corners with opening angles $\alpha = \pi/n$; thus $0 < \alpha < \pi$. The streamline patterns of these flows are well known.

In analogy, we seek conical stagnation-point solutions of (8) in the form of the series expansion

$$F = F_0 + \rho^n F_n(\phi) + \rho^m F_m(\phi) + o(\rho^m), \quad 1 < n < m, \tag{14}$$

where F_0 is a constant, which is irrelevant in plane flow. In conical flow, however, F_0, which equals the non-dimensionalized radial velocity component in the conical stagnation point (equation (5)), enters in the conical streamline pattern (equation (6)). As a result, depending on its magnitude, it may have a significant effect on this streamline pattern. In this paper we only consider supersonic conical stagnation points, so that $a_0 < |F_0| < 1$, where a_0 is the speed of sound in the conical stagnation point. It may be useful to remark that positive and negative values of F_0 are allowed in the present analysis; in most practical flow situations, however, $F_0 > 0$.

If (14) is substituted into (8) and the result ordered with respect to powers in ρ, the coefficient of the lowest-order term appears to be

$$F_n'' + n^2 F_n = 0, \tag{15}$$

with the solutions

$$F_n(\phi) = a_n \cos(n\phi + \psi_n), \quad n > 1, \tag{16}$$

where a_n and ψ_n are arbitrary constants. Thus this term exactly equals the stagnation-point solution for plane flow (see (13)). We may use the freedom, still existing in the choice of the co-ordinate system, to rotate the co-ordinate system around the x axis such that $\psi_n = 0$ in (16). When the next-higher-order terms are written out, several cases for n and m have to be distinguished. After equating the coefficient of the next-highest-order term to zero we obtain the following:

For $1 < n < 2$:

$$F_m'' + m^2 F_m = 0, \quad n < m < 3n-2, \tag{17}$$

$$F_m'' + m^2 F_m = n^3(n-1)a_0^{-2} F_n^3 + n(n-1)a_0^{-2} F_n (F_n')^2, \quad m = 3n-2, \tag{18}$$

$$n(n-1)F_n[n^2 F_n^2 + (F_n')^2] = 0, \quad m > 3n-2, \tag{19}$$

with the solutions

$$F_m(\phi) = b_m \cos(m\phi + \psi_m), \quad n < m < 3n-2, \tag{20}$$

$$F_m(\phi) = b_m \cos(m\phi + \psi_m) + \frac{n^3 a_n^3}{4a_0^2(2n-1)} \cos n\phi, \quad m = 3n-2, \tag{21}$$

whereas (19), when (16) is used, yields $F_n(\phi) \equiv 0$, which means that $m > 3n-2$ cannot occur. In (20) and (21) b_m and ψ_m are arbitrary constants.

For $n = 2$:

$$F_m'' + m^2 F_m = 0, \quad 2 < m < 4, \tag{22}$$

$$F_m'' + m^2 F_m = -2[1 - a_0^{-2}(F_0 - 2F_2)^2]F_2 - 2a_0^{-2}(F_0 - F_2)(F_2')^2, \quad m = 4, \tag{23}$$

$$F_2[a_0^2 - (F_0 - 2F_2)^2] + (F_0 - F_2)(F_2')^2 = 0, \quad m > 4, \tag{24}$$

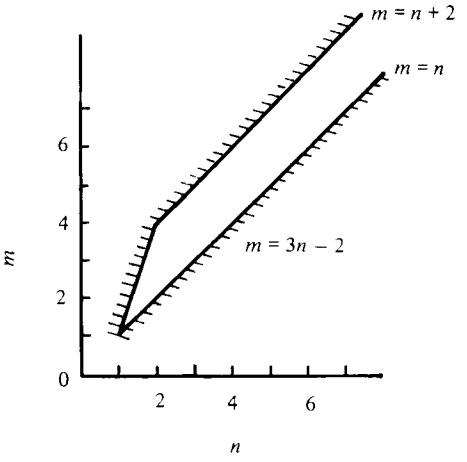

FIGURE 1. Values of n and m for which $F_n(\phi)$ and $F_m(\phi)$ exist.

with the solutions

$$F_m(\phi) = b_m \cos(m\phi + \psi_m), \quad 2 < m < 4, \tag{25}$$

$$F_m(\phi) = b_m \cos(m\phi + \psi_m) - \frac{a_2^2 F_0}{2a_0^2} - \frac{a_2(a_0^2 - F_0^2 - 4a_2^2)}{6a_0^2} \cos 2\phi, \quad m = 4, \tag{26}$$

whereas (24), when (16) is used, yields $F_2(\phi) \equiv 0$, which indicates that $m > 4$ cannot occur. In (25), (26) b_m and ψ_m are arbitrary constants.

For $n > 2$:

$$F_m'' + m^2 F_m = 0, \quad n < m < n+2, \tag{27}$$

$$F_m'' + m^2 F_m = -\left(1 - \frac{F_0^2}{a_0^2}\right) n(n-1) F_n, \quad m = n+2, \tag{28}$$

$$n(n-1)(a_0^2 - F_0^2) F_n = 0, \quad m > n+2, \tag{29}$$

with the solutions

$$F_m(\phi) = b_m \cos(m\phi + \psi_m), \quad n < m < n+2, \tag{30}$$

$$F_m(\phi) = b_m \cos(m\phi + \psi_m) - \frac{n(n-1)}{m^2 - n^2} a_n \left(1 - \frac{F_0^2}{a_0^2}\right) \cos n\phi, \quad m = n+2, \tag{31}$$

whereas (29), when (16) is used, yields $F_n(\phi) \equiv 0$, which means that $m > n+2$ cannot occur. In (30), (31) b_m and ψ_m are arbitrary constants. Figure 1 shows the values of n and m for which it is possible to determine the functions $F_n(\phi)$ and $F_m(\phi)$ in the expansion given by (14). With the aid of the listed solutions for the conical velocity potential and (6) or (9) the conical streamline pattern near the conical stagnation point may be determined. The pressure distribution follows from the relation

$$\left(\frac{p}{p_0}\right)^{(\gamma-1)/\gamma} = \left(\frac{a}{a_0}\right)^2 = \frac{1 - (u^2 + v^2 + w^2)}{1 - u_0^2}, \tag{32}$$

where the zero subscript indicates conditions in the conical stagnation point.

3. Conical streamline pattern and pressure distribution near a conical stagnation point in potential flow

3.1. *Case* $1 < n < 2$: *oblique saddle points*

Substitution of (16), (20), (21) into (14), and (14) into (9), leads to the equation for the conical streamlines

$$\frac{d\rho}{d\phi} = \frac{na_n\rho^{n+1}\cos n\phi - F_0\,\rho^3 + O(\rho^{m+1})}{-na_n\rho^n \sin n\phi + O(\rho^m)}. \tag{33}$$

Introducing a parameter τ along the streamlines, we investigate (33) as a system in the (ϕ, ρ) plane. Then

$$\left.\begin{aligned} \frac{d\phi}{d\tau} &= -\sin n\phi + O(\rho^{m-n}), \\ \frac{d\rho}{d\tau} &= \rho\cos n\phi - \frac{F_0}{na_n}\rho^{3-n} + O(\rho^{m-n+1}). \end{aligned}\right\} \tag{34}$$

The singular points of this system for $\rho = 0$ are in $\phi = k\pi/n$ ($k = 0, \pm 1, \pm 2, \ldots$), which appear to be saddle points for the locally linearized system. It may be shown that the higher-order terms do not change the saddle-point character of these singular points (Andronov *et al.* 1973). Retaining only the lowest-order terms in (34) yields, upon integration, the approximate shape of the conical streamlines

$$\rho^n \sin n\phi = C, \tag{35}$$

where C is constant along a streamline. It is well known that (35) also represents the streamlines in an incompressible stagnation-point flow. Equation (35) represents the streamline pattern for a flow in a corner with an including angle $\alpha = \pi/n$; thus $\pi/2 < \alpha < \pi$ for $1 < n < 2$. Obviously, it is not possible to fill out a full neighbourhood ($0 \leqslant \phi < 2\pi$) of the conical stagnation point with corner flows, such that the velocity is continuous. The conical stagnation point can therefore only occur on a body surface, with one or more streamlines coinciding with the body surface.

From (7) and (14) the velocity components may be obtained as

$$\left.\begin{aligned} u &= F_0 - (n-1)a_n\rho^n\cos n\phi + O(\rho^m), \\ v &= na_n\rho^{n-1}\cos(n-1)\phi + O(\rho^{m-1}), \\ w &= -na_n\rho^{n-1}\sin(n-1)\phi + O(\rho^{m-1}). \end{aligned}\right\} \tag{36}$$

The pressure distribution then follows from (32) and (36)

$$\left(\frac{p}{p_0}\right)^{(\gamma-1)/\gamma} = 1 - \frac{n^2a_n^2}{1-F_0^2}\rho^{2n-2} + O(\rho^{n+m-2}). \tag{37}$$

The pressure attains a maximum in the conical stagnation point, and the isobars are to a first approximation concentric circles around the origin. In figure 2(*a*) the streamline pattern in a corner $k\pi/n < \phi < (k+1)\pi/n$ is shown. The direction of flow on these streamlines corresponds to $a_n\cos k\pi < 0$; if $a_n\cos k\pi > 0$ the flow direction should be reversed. This follows from (11), (14), (16), (20), (21) which yield

$$x\frac{d\rho}{dt} = na_n\rho^{n-1}\cos n\phi - F_0\,\rho + O(\rho^{m-1}). \tag{38}$$

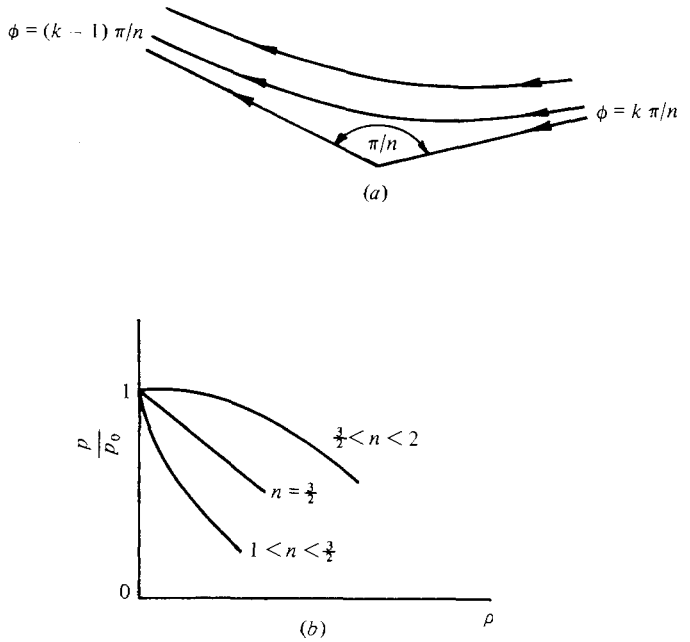

FIGURE 2. Oblique saddle point ($1 < n < 2$); (*a*) conical flow in a corner with angle π/n, $a_n \cos k\pi < 0$; (*b*) pressure distribution near corner point.

Figure 2(*b*) gives the pressure distribution for various values of n, as obtained from (37). It appears that the pressure gradient at the conical stagnation point is singular for $1 < n < \frac{3}{2}$.

3.2. *Case* $n = 2$

Substitution of (16), (25), (26) into (14), and (14) into (6), leads to the equation for the conical streamlines

$$\frac{d\zeta}{d\eta} = \frac{-(2a_2+F_0)\zeta + (mF_m \sin\phi + F'_m \cos\phi)\rho^{m-1} + a_2\rho^3 \sin\phi\cos 2\phi + O(\rho^{m+1})}{(2a_2-F_0)\eta + (mF_m \cos\phi - F'_m \sin\phi)\rho^{m-1} + a_2\rho^3 \cos\phi\cos 2\phi + O(\rho^{m+1})}. \tag{39}$$

When (39) is written as a system and only the linear terms are retained, there follows

$$\frac{d\eta}{d\tau} = (-1+2\lambda)\eta, \quad \frac{d\zeta}{d\tau} = (-1-2\lambda)\zeta, \tag{40}$$

where $\lambda = a_2 F_0^{-1}$. The eigenvalues of the coefficient matrix are therefore

$$\mu_{1,2} = -1 \pm 2\lambda. \tag{41}$$

We are thus led to distinguish between the cases $|\lambda| = \frac{1}{2}$ and $|\lambda| \neq \frac{1}{2}$.

3.2.1. *Case* $|\lambda| \neq \frac{1}{2}$: *nodes and saddle points*

In this case none of the eigenvalues $\mu_{1,2}$ is equal to zero and the solutions of (40) may be expected to give an approximation of the streamline pattern near the conical stagnation point. Equations (25), (26), however, show that for $2 < m < 3$, $3 < m < 4$ the function $F_m(\phi)$ is not periodic with period 2π; therefore it is not possible to fill out

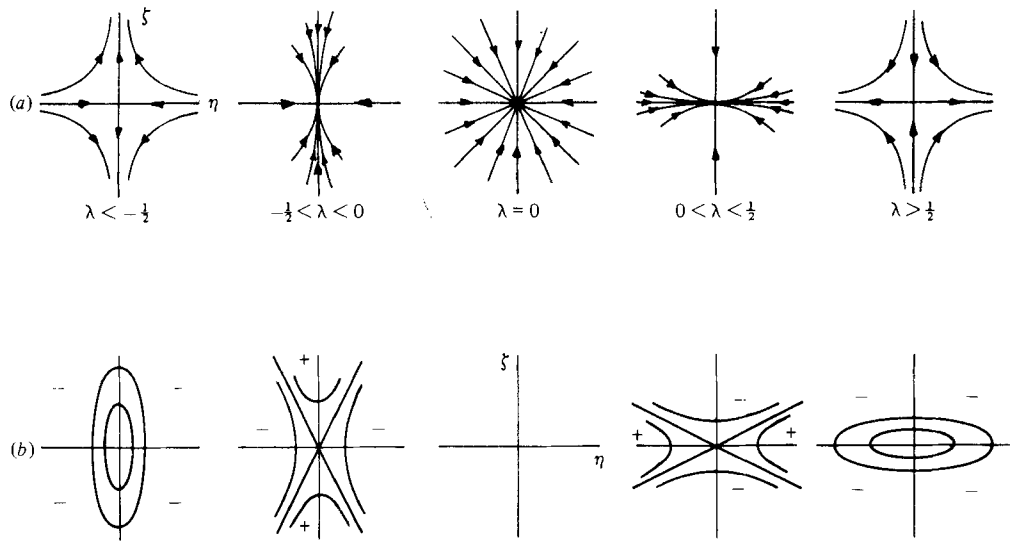

FIGURE 3. Saddle points, nodes and starlike node ($n = 2$, $|\lambda| \neq \frac{1}{2}$, $m = 3$ or 4); (a) conical streamlines; (b) isobars.

a full neighbourhood of the stagnation point such that the velocity is continuous. For $2 < m < 3$ and $3 < m < 4$ parts of the solutions between streamlines may be used to construct flows near conical stagnation points on a body surface. If $m = 3$ or $m = 4$ the behaviour of $F_m(\phi)$ allows the conical stagnation point to appear in the flow field away from a body surface. If this remains true when all higher-order terms are added, the point can be realized in the flow, and the character of the singularity in the streamline pattern is determined by (40) (Coddington & Levinson 1955). The singularity of (40) is a starlike node for $\lambda = 0$, and a node with two perpendicular approach directions for the streamlines for $0 < |\lambda| < \frac{1}{2}$, whereas it is a saddle point with orthogonal separatrices for $|\lambda| > \frac{1}{2}$. It may be observed that a large value of $|\lambda|$ corresponds to a value of F_0 ($F_0 = u_0$ = radial velocity in the conical stagnation point) which is small compared to a_2, and represents that part of the solution which also occurs in the incompressible flow near a stagnation point. The flow pattern then resembles that of the incompressible plane flow. If $|\lambda|$ is decreased, the radial velocity becomes more dominant such that for $|\lambda| < \frac{1}{2}$ the streamline pattern forms a node, which is not observed in incompressible plane flow. Sketches of the conical streamline pattern are given in figure 3 for $F_0 > 0$; for $F_0 < 0$ the direction of the streamlines is reversed. The flow direction may be obtained from

$$\left.\begin{aligned} x\frac{d\eta}{dt} &= 2F_0(\lambda - \tfrac{1}{2})\eta + O((\eta^2+\zeta^2)^{\frac{1}{2}}), \\ x\frac{d\zeta}{dt} &= -2F_0(\lambda + \tfrac{1}{2})\zeta + O((\eta^2+\zeta^2)^{\frac{1}{2}}), \end{aligned}\right\} \tag{42}$$

which may be derived from (10), (5), (14).

From (7), (14) the velocity components may be obtained:

$$\left.\begin{aligned} u &= F_0 - a_2\rho^2\cos 2\phi - (m-1)\rho^m F_m + o(\rho^m),\\ v &= 2a_2\rho\cos\phi + (mF_m\cos\phi - F_m'\sin\phi)\rho^{m-1} + o(\rho^{m-1}),\\ w &= -2a_2\rho\sin\phi + (mF_m\sin\phi + F_m'\cos\phi)\rho^{m-1} + o(\rho^{m-1}). \end{aligned}\right\} \tag{43}$$

The pressure distribution then follows from (32), (43):

$$\left(\frac{p}{p_0}\right)^{(\gamma-1)/\gamma} = 1 - \frac{4\lambda F_0^2}{1-F_0^2}[(\lambda-\tfrac{1}{2})\eta^2 + (\lambda+\tfrac{1}{2})\zeta^2] + O(\rho^m). \tag{44}$$

If $|\lambda| > \frac{1}{2}$, and thus when a saddle point singularity for the streamlines occurs, the pressure attains a maximum in the conical stagnation point and the isobars are to a first approximation concentric ellipses around the origin. Again the similarity with the incompressible case (and the case $1 < n < 2$) is obvious. If $0 < |\lambda| < \frac{1}{2}$ – the streamlines then have a nodal singularity – the isobars are to a first approximation concentric hyperbolae with asymptotes given by

$$\zeta = \pm\left(\frac{\frac{1}{2}-\lambda}{\frac{1}{2}+\lambda}\right)^{\frac{1}{2}}\eta. \tag{45}$$

In the regions within the acute angle between the asymptotes the pressure is higher than in the conical stagnation point, whereas in the other regions the pressure is lower. Comparison of the isobars with the streamline pattern shows that, in the direction along which an infinite number of streamlines approach, the pressure shows a minimum at the conical stagnation point, whereas, in the direction along which only one streamline approaches, the pressure reaches a maximum. For $\lambda = 0$ the pressure does not change to the order $m\gamma/(\gamma-1)$ of the distance from the conical stagnation point; this case actually corresponds to $n > 2$ and will be further discussed in § 3.3.

3.2.2. *Case* $|\lambda| = \frac{1}{2}$: *saddle-nodes, topological saddle points, topological nodes*†

If $|\lambda| = \frac{1}{2}$, one of the eigenvalues $\mu_{1,2}$ given by (41) is equal to zero and the nonlinear terms in (39) cannot be neglected when considering the streamline pattern. From (39) it is clear that we should distinguish two cases: $2 < m < 4$ and $m = 4$.

(*a*) $2 < m < 4$. For $\lambda = \pm\frac{1}{2}$ equations (14), (16), (25) show that the conical potential may be written as:

$$F = F_0[1 \pm \tfrac{1}{2}\rho^2\cos 2\phi + \frac{2\mu}{m}\rho^m\cos(m\phi + \psi_m) + o(\rho^m)], \tag{46}$$

where $\mu = mb_m/2F_0$. We restrict ourselves to $\lambda = -\frac{1}{2}$; the case $\lambda = \frac{1}{2}$ may be obtained by retaining the minus sign in (46) and replacing ϕ and ψ_m by $\phi + \pi/2$ and $\psi_m - \frac{1}{2}m\pi$, respectively. Substitution of (46) into (9) leads to the equation for the conical streamlines

$$\frac{d\rho}{d\phi} = \frac{-\rho\cos^2\phi + \mu\rho^{m-1}\cos(m\phi+\psi_m) + O(\rho^3)}{\sin\phi\cos\phi - \mu\rho^{m-2}\sin(m\phi+\psi_m) + o(\rho^{m-2})}. \tag{47}$$

Using the parameter τ along the streamlines, we investigate (47) as a system in the (ϕ, σ) plane, where $\sigma = \rho^{m-2}$ $(\sigma \geqslant 0)$. Then

$$\left.\begin{aligned} \frac{d\phi}{d\tau} &= \sin\phi\cos\phi - \mu\sigma\sin(m\phi+\psi_m) + o(\sigma),\\ \frac{d\sigma}{d\tau} &= -(m-2)\sigma\cos^2\phi + (m-2)\mu\sigma^2\cos(m\phi+\psi_m) + O(\sigma^{m/(m-2)}). \end{aligned}\right\} \tag{48}$$

† The terminology for these multiple singular points follows that used in Andronov *et al.* (1973).

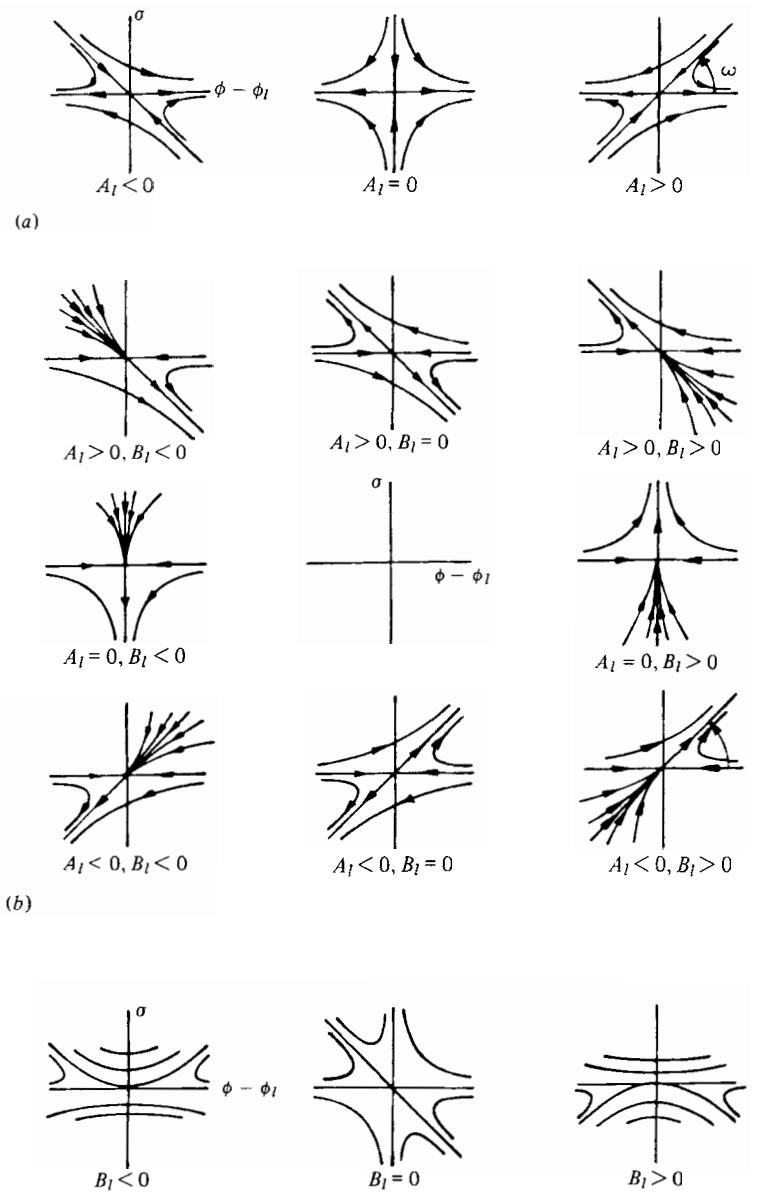

FIGURE 4. Conical streamlines and isobars in the $(\phi-\phi_l,\sigma)$ plane ($n = 2, \lambda = -\frac{1}{2}, 2 < m < 4$). (*a*) Flow near $\phi = \phi_l = \frac{1}{2}\pi l$, $l = 0, \pm 2, \pm 4, \ldots$. (*b*) Flow near $\phi = \phi_l = \frac{1}{2}\pi l$, $l = \pm 1, \pm 3, \ldots$. (*c*) Isobars near $\phi = \phi_l = \frac{1}{2}\pi l$, $l = \pm 1, \pm 3, \ldots$.

The singular points of this system for $\sigma = 0$ are in $\phi = \phi_l = \frac{1}{2}l\pi$ ($l = 0, \pm 1, \pm 2, \ldots$). Expanding with respect to $\phi - \phi_l$ and retaining only terms up to second order yields from (48)

$$\left.\begin{aligned} \frac{d\phi}{d\tau} &= ab + (-a^2+b^2)(\phi-\phi_l) - A_l\sigma - 2ab(\phi-\phi_l)^2 - mB_l(\phi-\phi_l)\sigma, \\ \frac{d\sigma}{d\tau} &= -(m-2)b^2\sigma + 2(m-2)ab(\phi-\phi_l)\sigma + (m-2)B_l\sigma^2, \end{aligned}\right\} \tag{49}$$

where $a = \sin\phi_l$, $b = \cos\phi_l$, $A_l = \mu\sin(m\phi_l + \psi_m)$, $B_l = \mu\cos(m\phi_l + \psi_m)$. There are two cases: l even, $a = 0$, $b^2 = 1$ and l odd, $a^2 = 1$, $b = 0$. If (49) is linearized the eigenvalues of the coefficient matrix are given by

$$\mu_1 = -a^2 + b^2, \quad \mu_2 = -(m-2)\,b^2. \tag{50}$$

If l is even, $\phi = \phi_l$, $\sigma = 0$ is a saddle point, also for the nonlinear system (49). Sketches of the streamline pattern in the $(\phi - \phi_l, \sigma)$ plane are given in figure 4 (*a*). The separatrices make an angle ω with the $(\phi - \phi_l)$ axis, where $\omega = 0$ or $\tan^{-1}\{(m-1)\,A_l^{-1}\}$. The flow direction corresponds to $F_0 > 0$. It should be noted that only $\sigma \geqslant 0$ is of interest for the present investigation. If l is odd, (50) yields $\mu_1 = -1$, $\mu_2 = 0$ and higher-order terms cannot be neglected. Expanding (48) and retaining only terms to third order yields

$$\left.\begin{aligned} \frac{d\phi}{d\tau} &= -(\phi - \phi_l) - A_l\sigma - mB_l(\phi - \phi_l)\,\sigma, \\ \frac{d\sigma}{d\tau} &= (m-2)\,B_l\sigma^2 - (m-2)\,(\phi - \phi_l)^2\sigma - m(m-2)\,A_l(\phi - \phi_l)\,\sigma^2. \end{aligned}\right\} \tag{51}$$

For $\phi = \phi_l$, $\sigma = 0$ system (51) has a multiple equilibrium point with $\mu_1 + \mu_2 = -1$. This permits us to follow the line of analysis given by Andronov *et al.* (1973, pp. 337–346).

Take first $A_l \neq 0$. Then, by the change of variables

$$\phi^* = -(\phi - \phi_l) - A_l\sigma, \quad \sigma^* = -A_l\sigma \quad \text{and} \quad \tau^* = -\tau,$$

we obtain from (51)

$$\left.\begin{aligned} \frac{d\phi^*}{d\tau^*} &= \phi^* - m\frac{B_l}{A_l}\phi^*\sigma^* + 2(m-1)\frac{B_l}{A_l}\sigma^{*2} + O((\phi^{*2} + \sigma^{*2})^{\frac{3}{2}}), \\ \frac{d\sigma^*}{d\tau^*} &= (m-2)\frac{B_l}{A_l}\sigma^{*2} + O((\phi^{*2} + \sigma^{*2})^{\frac{3}{2}}), \end{aligned}\right\} \tag{52}$$

from which follows that $d\phi^*/d\tau^* = 0$ on the curve

$$\phi^* = f(\sigma^*) = -2(m-1)\frac{B_l}{A_l}\sigma^{*2} + O(\sigma^{*3}), \tag{53}$$

and that on this curve

$$\frac{d\sigma^*}{d\tau^*} = \Delta_k\sigma^{*k} + O(\sigma^{*k+1}) = (m-2)\frac{B_l}{A_l}\sigma^{*2} - (m-1)\,(m-2)\,\sigma^{*3} + O(\sigma^{*4}). \tag{54}$$

For $B_l \neq 0$, there follows $k = 2$, and, according to theorem 65 in Andronov *et al.* (1973, p. 340), the equilibrium point is a saddle-node. It has one parabolic (nodal type) sector and two hyperbolic (saddle-point type) sectors. If $B_l/A_l < 0$ the hyperbolic sectors contain a segment of the positive σ^* axis and if $B_l/A_l > 0$ they contain a segment of the negative σ^* axis. For $B_l = 0$, there follows $k = 3$, $\Delta_k < 0$ and the equilibrium point is a topological saddle point, whose separatrices are directed along the ϕ^*, σ^* axes.

For $A_l \neq 0$ the streamline pattern may now be sketched in the $(\phi - \phi_l, \sigma)$ plane as is done in figure 4 (*b*). The separatrices include an angle ω with the $(\phi - \phi_l)$ axis, where $\omega = 0$ or $\tan^{-1}A_l^{-1}$, the latter value also indicating the approach direction for streamlines in a nodal part of the singularity. The flow directions in figure 4 (*b*) correspond to $F_0 > 0$. It should be noted that only $\sigma \geqslant 0$ is of interest for the present investigation.

Now take $A_l = 0$. Since $A_l^2 + B_l^2 = \mu^2$, and $\mu = 0$ cannot occur in the proposed expansion given in (46), $A_l = 0$ implies $B_l \neq 0$. Then, by the change of variables $\phi^* = \phi - \phi_l$, $\sigma^* = \sigma$ and $\tau^* = -\tau$, (51) becomes

$$\left.\begin{aligned} \frac{d\phi^*}{d\tau^*} &= \phi^* + mB_l\phi^*\sigma^*, \\ \frac{d\sigma^*}{d\tau^*} &= -(m-2)B_l\sigma^{*2} + O((\phi^{*2}+\sigma^{*2})^{\frac{3}{2}}), \end{aligned}\right\} \tag{55}$$

from which it follows that $d\phi^*/d\tau^* = 0$ on the curve

$$\phi^* = f(\sigma^*) \equiv 0, \tag{56}$$

and that on this curve:

$$\frac{d\sigma^*}{d\tau^*} = \Delta_k\sigma^{*k} + O(\sigma^{*k+1}) = -(m-2)B_l\sigma^{*2} + O(\sigma^{*3}). \tag{57}$$

Thus, since $k = 2$, the equilibrium point is a saddle-node. If $B_l > 0$, the hyperbolic sectors contain a segment of the positive σ^* axis, if $B_l < 0$a segment of the negative σ^* axis. The streamline pattern in the $(\phi - \phi_l, \sigma)$ plane for $A_l = 0$ is also sketched, figure 4 (*b*).

The possible streamline patterns near $\phi = \phi_l$, as described above, may now be used to determine the streamline patterns in the (η, ζ) plane. Obviously, only in the case $m = 3$ the behaviour of $F_m(\phi)$ allows the conical stagnation point to appear in a flow field away from a body surface. If higher-order terms permit, we may then derive the following streamline pattern for such a conical stagnation point. We restrict the range of ϕ to $0 \leqslant \phi < 2\pi$, thus $\phi_0 = 0$, $\phi_1 = \frac{1}{2}\pi$, $\phi_2 = \pi$, $\phi_3 = \frac{3}{2}\pi$. If $\phi = \phi_0 (= 0)$ or $\phi_2 (= \pi)$ there is only one streamline approaching the stagnation point and for $F_0 > 0$ the streamline is directed towards this point. If $\phi = \phi_1 (= \frac{1}{2}\pi)$ or $\phi_3 (\frac{3}{2}\pi)$ there are two possibilities: there is either only one streamline approaching the stagnation point and for $F_0 > 0$ this streamline flows away from this point ($B_l \geqslant 0$), or there are an infinite number of streamlines flowing towards the stagnation point ($F_0 > 0$, $B_l < 0$). Since, moreover, for $m = 3$, $B_1 = -B_3$, there are three possibilities: (i) $B_1 < 0$, $B_3 > 0$, (ii) $B_1 = 0$, $B_3 = 0$, (iii) $B_1 > 0$, $B_3 < 0$. This leads to two types of streamline patterns: (1) topological saddle points ($B_1 = B_3 = 0$), (2) saddle-nodes ($B_1 \neq 0, B_3 \neq 0$). Sketches of these flow patterns are given in figure 5 (*a*) with flow directions corresponding to $F_0 > 0$.

If $2 < m < 3$, $3 < m < 4$ equation (46) shows that it is not possible to fill out a full neighbourhood of the conical stagnation point with these solutions, such that the velocity is continuous. Parts of these solutions may be used, however, to construct flows near a conical stagnation point on a body surface. It may easily be seen that the maximum sector through which such a solution can be extended is equal to $\frac{3}{2}\pi$; without loss of generality we may take $0 \leqslant \phi \leqslant \frac{3}{2}\pi$. From figure 4 it may become apparent that four relevant combinations of B_1 and B_3 can be made: (i) $B_1 < 0$, $B_3 < 0$, (ii) $B_1 < 0$, $B_3 \geqslant 0$, (iii) $B_1 \geqslant 0$, $B_3 < 0$, (iv) $B_1 \geqslant 0$, $B_3 \geqslant 0$. The corresponding streamline patterns for $F_0 > 0$ are shown in figure 6 (*a*). They may be called a partial topological node, a partial saddle-node, a partial topological saddle-node and a partial topological saddle, respectively.

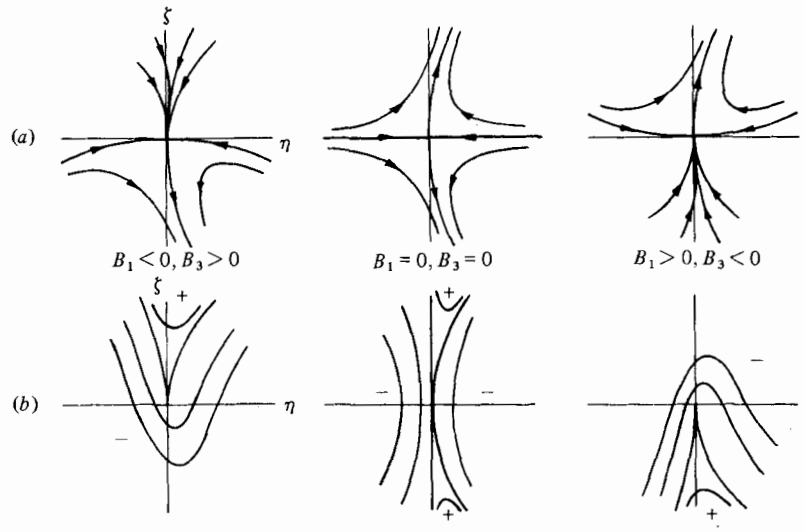

FIGURE 5. Saddle-nodes and topological saddle ($n = 2$, $\lambda = -\frac{1}{2}$, $m = 3$); (*a*) conical streamlines; (*b*) isobars.

We now come to the determination of the isobars corresponding to the established streamline patterns. From (7), (46) the velocity components may be obtained as

$$\left.\begin{aligned} u &= u_0[1+\tfrac{1}{2}\rho^2\cos 2\phi - 2\frac{m-1}{m}\mu\rho^m\cos(m\phi+\psi_m)+o(\rho^m)],\\ v &= u_0[-\rho\cos\phi + 2\mu\rho^{m-1}\cos\{(m-1)\phi+\psi_m\}+o(\rho^{m-1})],\\ w &= u_0[\rho\sin\phi - 2\mu\rho^{m-1}\sin\{(m-1)\phi+\psi_m\}+o(\rho^{m-1})], \end{aligned}\right\} \tag{58}$$

and for the pressure distribution there follows

$$\left(\frac{p}{p_0}\right)^{(\gamma-1)/\gamma} = 1-\frac{2u_0^2}{1-u_0^2}G(\phi,\rho)+o(\rho^m), \tag{59}$$

where $G(\phi,\rho) = \rho^2\cos^2\phi - 2\mu\rho^m[2\cos\phi\cos\{(m-1)\phi+\psi_m\}-(1/m)\cos(m\phi+\psi_m)]$. The isobars are, in first approximation, given by the lines G = constant, which are easier to analyse as solutions of the differential equation

$$\left(\frac{d\rho}{d\phi}\right)_{G=\text{constant}} = -\frac{\partial G/\partial\phi}{\partial G/\partial\rho} = \frac{\rho\sin\phi\cos\phi+\mu\rho^{m-1}f'(\phi)}{\cos^2\phi-\mu m\rho^{m-2}f(\phi)}, \tag{60}$$

where

$$f(\phi) = 2\cos\phi\cos[(m-1)\phi+\psi_m]-\frac{1}{m}\cos(m\phi+\psi_m). \tag{61}$$

Introducing a parameter τ along the isobars, we may investigate (60) as a system in the (ϕ,σ) plane, where $\sigma = \rho^{m-2}$ ($\sigma \geqslant 0$). Then

$$\left.\begin{aligned} \frac{d\phi}{d\tau} &= \cos^2\phi-\mu m\sigma f(\phi),\\ \frac{d\sigma}{d\tau} &= (m-2)\sigma\sin\phi\cos\phi+\mu(m-2)\sigma^2 f'(\phi). \end{aligned}\right\} \tag{62}$$

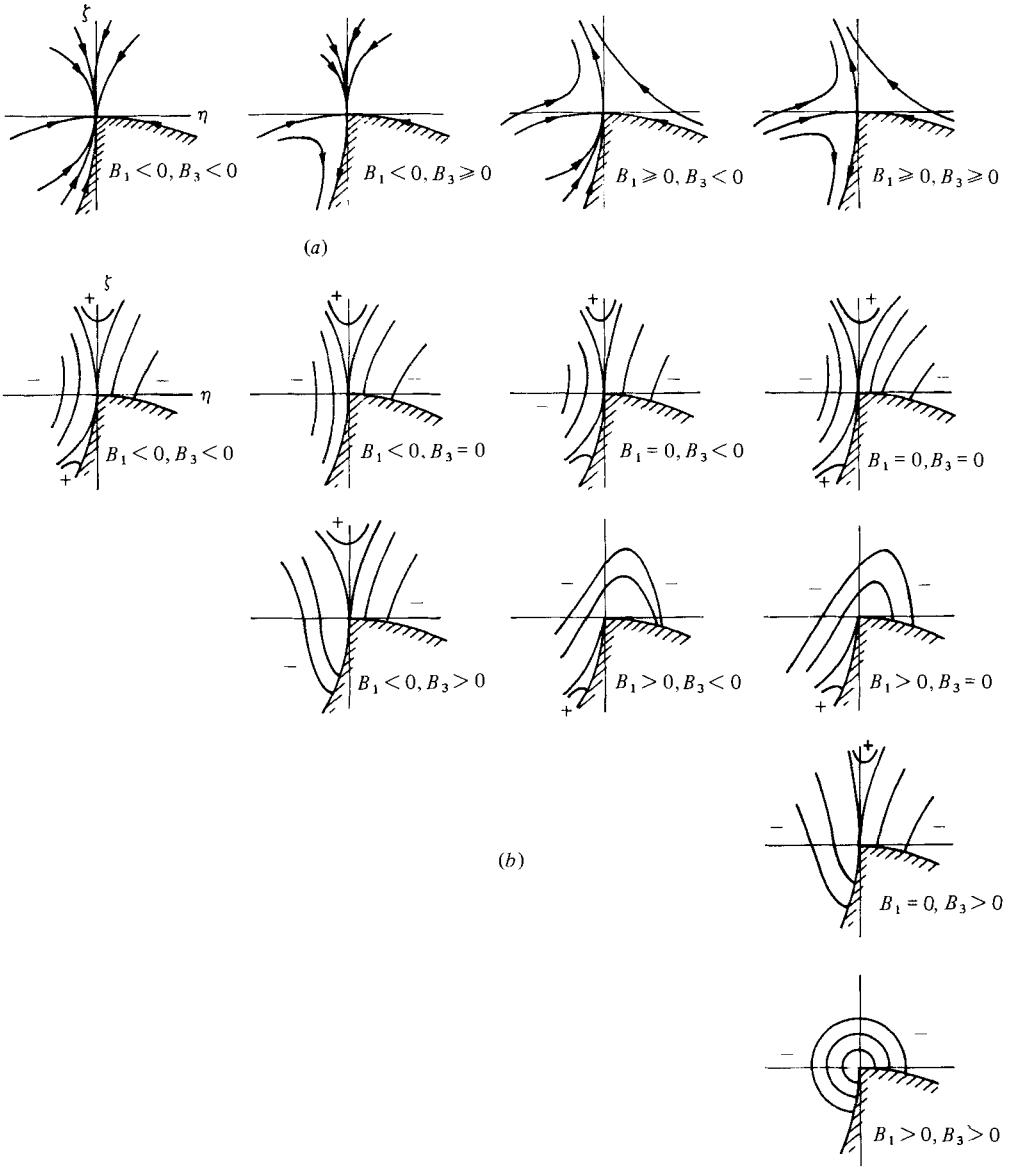

FIGURE 6. Partial topological node, partial saddle-nodes, partial topological saddle ($n = 2$, $\lambda = -\frac{1}{2}$, $2 < m < 4$, $m \neq 3$). (*a*) Conical streamlines. (*b*) Isobars.

The singular points of this system for $\sigma = 0$ are in $\phi = \phi_l = \frac{1}{2}l\pi$ ($l = \pm 1, \pm 3, \ldots$). Expanding with respect to $\phi - \phi_l$ and retaining terms to the third order yields

$$\left.\begin{aligned} \frac{d\phi}{d\tau} &= B_l\sigma + m\,A_l\sigma(\phi-\phi_l) + (\phi-\phi_l)^2 - \tfrac{1}{2}m(4-3m)\,B_l\sigma(\phi-\phi_l)^2, \\ \frac{d\sigma}{d\tau} &= -(m-2)\,A_l\sigma^2 - (m-2)\,\sigma(\phi-\phi_l) + (m-2)\,(4-3m)\,B_l\sigma^2(\phi-\phi_l). \end{aligned}\right\} \tag{63}$$

For $B_l \neq 0$ the eigenvalues of the linearized system are equal to zero and, as before,

we will follow the line of analysis given in Andronov *et al.* (1973, pp. 346–369), to investigate the integral paths of (63). For that purpose we divide the right-hand sides of (63) by B_l. For the curve on which $d\phi/d\tau = 0$ may be found

$$\sigma = -\frac{1}{B_l}(\phi-\phi_l)^2 + O((\phi-\phi_l)^3), \tag{64}$$

and on this curve there is

$$\frac{d\sigma}{d\tau} = \Delta_k(\phi-\phi_l)^k + O\{(\phi-\phi_l)^{k+1}\} = \frac{m-2}{B_l^2}(\phi-\phi_l)^3 + O\{(\phi-\phi_l)^4\}. \tag{65}$$

Hence, it follows that $k = 3$ and theorem 66 in Andronov *et al.* (1973, p. 357) may be applied. As a result the equilibrium point appears to be a topological saddle point. Sketches of the isobars in the $(\phi-\phi_l, \sigma)$ plane are given in figure 4(*c*).

For $B_l = 0$, (63) may be integrated to yield

$$(2A_l\sigma + \phi - \phi_l)\,\sigma^{2/(m-2)}(\phi-\phi_l) = C, \tag{66}$$

where C is constant along an isobar. The isobars for this case are also given in figure 4(*c*). The singularity involves six hyperbolic sectors and separatrices along the $(\phi-\phi_l)$ axis, the σ axis and the line $\sigma = -(\phi-\phi_l)/2A_l$ ($A_l \neq 0$ since $B_l = 0$ and $A_l^2 + B_l^2 \neq 0$). It should be noted that only $\sigma \geqslant 0$ is of interest in this investigation.

The isobar patterns in the $(\phi-\phi_l, \sigma)$ plane near $\phi = \phi_l$, as described above, may now be used to determine the isobars in the (η, ζ) plane. For $m = 3$ these isobar patterns are sketched in figure 5(*b*), and two types are encountered: (i) a degenerated saddle point $B_1 \neq 0$, $B_3 \neq 0$, (ii) a topological saddle point $B_1 = B_3 = 0$. For $2 < m < 4$ ($m \neq 3$) the isobar patterns are sketched in figure 6(*b*). In figures 5(*b*) and 6(*b*) regions with a pressure higher than in the stagnation point are indicated by a plus sign, whereas a lower pressure is indicated by a minus sign.

(*b*) $m = 4$. For $\lambda = \pm\frac{1}{2}$ equations (14), (16), (26) show that the conical potential may be written as

$$F = F_0[1 \pm \tfrac{1}{2}\rho^2\cos 2\phi + \rho^4\{\tfrac{1}{2}\mu\cos(4\phi+\psi_4) - \tfrac{1}{8}M_0^2 \mp \tfrac{1}{12}(1-2M_0^2)\cos 2\phi\} + o(\rho^4)], \tag{67}$$

where $\mu = mb_m/2F_0 = 2b_4/F_0$, and $M_0 = F_0/a_0$ is the Mach number in the conical stagnation point. We restrict ourselves to $\lambda = -\frac{1}{2}$, since the results for $\lambda = +\frac{1}{2}$ may be obtained by replacing ϕ by $\phi + \frac{1}{2}\pi$ while retaining the lower sign in (67). Substitution of (67) into (6) leads to the equation for the streamlines

$$\frac{d\zeta}{d\eta} = \frac{-2\alpha\eta^3 - 3\beta\eta^2\zeta + 6\alpha\eta\zeta^2 + \beta\zeta^3 + o(\rho^3)}{-2\eta + \sum_{k=0}^{3}\gamma_k\eta^{3-k}\zeta^k + o(\rho^3)}, \tag{68}$$

where α, β and γ_k are constants depending on M_0, μ and ψ_4. Since the point $\eta = \zeta = 0$ is a multiple equilibrium point, which may be analysed similarly to previous cases, only $\alpha = \mu\sin\psi_4$ and $\beta = \frac{1}{6}(1+M_0^2) + 2\mu\cos\psi_4$ are of importance for this analysis. Applying theorem 65 of Andronov *et al.* (1973, p. 340), we find that the point is a topological node for $\beta < 0$ and a topological saddle point for $\beta > 0$. For $\beta = 0$ and $\alpha \neq 0$, again a topological saddle point occurs. The case $\beta = 0$ and $\alpha = 0$ cannot be considered without taking into account higher-order terms in the expansion for F.

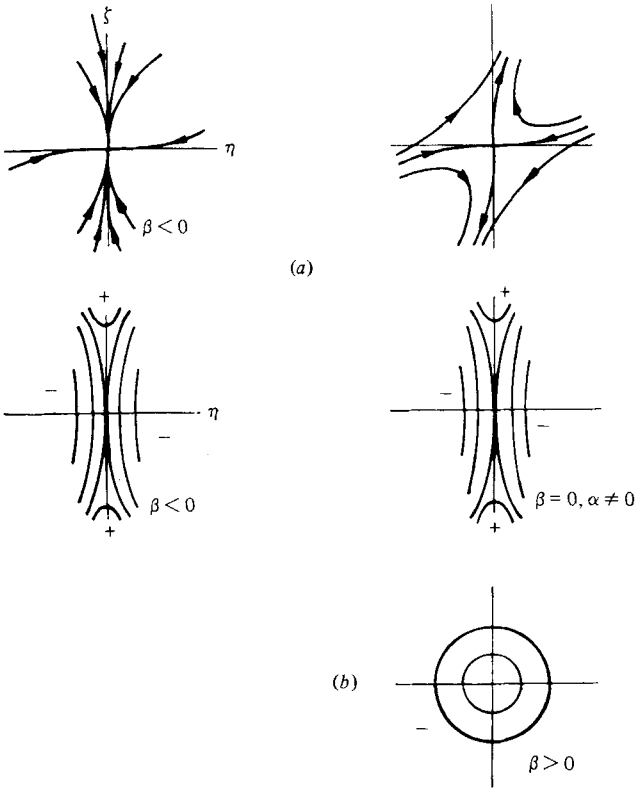

FIGURE 7. Topological node and topological saddle ($n = 2, \lambda = -\frac{1}{2}, m = 4$). (*a*) Conical streamlines. (*b*) Isobars.

The isobars are the integral paths of the differential equation

$$\frac{d\zeta}{d\eta} = \frac{\eta + \sum_{k=0}^{3} \delta_k \eta^{3-k} \zeta^k + o(\rho^3)}{-5\alpha\eta^3 + (1 - \frac{9}{2}\beta)\eta^2\zeta + 3\alpha\eta\zeta^2 - \frac{1}{2}\beta\zeta^3 + o(\rho^3)}, \tag{69}$$

where δ_k are constants depending on M_0, μ and ψ_4; they are not of importance for the analysis. Following again Andronov *et al.* (1973), theorem 66 (p. 357) yields that for $\beta < 0$ and for $\beta = 0$ but $\alpha \neq 0$ the isobars form a topological saddle point, whereas for $\beta > 0$ a centre point singularity occurs. Streamline patterns for $F_0 > 0$ and isobars are sketched in figure 7.

3.2.3. *Stability of the flow solutions for* $n = 2$

The singularities in the streamline patterns discussed in the previous sections can be divided into two classes. On the one hand there are the structurally stable singularities, corresponding to $|\lambda| \neq \frac{1}{2}$, and consisting of nodes and saddle points. They are structurally stable in the sense that small changes in the flow problem by changing the boundary conditions in general result in a small variation of λ, which leaves the character of the singularity invariant.

The second class of singularities, containing saddle-nodes, topological saddles and

topological nodes, is found for $|\lambda| = \frac{1}{2}$. These are structurally unstable; small changes will cause bifurcation, as a result of which the topological character of the streamline pattern changes (Andronov *et al.* 1971). This may occur by the generation of several singularities of the first class or the complete disappearance of the singularity.

3.3. *Case $n > 2$: star-like nodes*

Substitution of (16), (30), (31) into (14), and (14) into (9) leads to the equation for the conical streamlines

$$\frac{d\rho}{d\phi} = \frac{-F_0\rho^3 + na_n\rho^{n+1}\cos n\phi + O(\rho^{m+1})}{-na_n\rho^n \sin n\phi + O(\rho^m)}, \tag{70}$$

which, in fact, is equal to (33) for the case $1 < n < 2$. Comparison of (33) and (70), however, shows the dominant influence of the (radial) velocity component F_0 in the conical stagnation point in the case $n > 2$. Introducing the parameter τ along the streamlines, we investigate (70) as a system in the (ϕ, σ) plane, where $\sigma = \rho^{n-2}$ $(\sigma \geqslant 0)$. Then

$$\left.\begin{aligned} \frac{d\phi}{d\tau} &= -na_n \sin n\phi + O\left(\sigma^{(m-n)/(n-2)}\right), \\ \frac{d\sigma}{d\tau} &= -(n-2)F_0 + n(n-2)a_n\sigma\cos n\phi + O(\sigma^{1+(m-n)/(n-2)}). \end{aligned}\right\} \tag{71}$$

The line $\sigma \equiv 0$ thus contains only regular points of (71), as a result of which through any point of this line there exists a single integral curve of (71). Correspondingly, in the (η, ζ) plane, there is one and only one streamline approaching the origin in any direction within a sector near the conical stagnation point. It is natural from (70) to consider sectors with an opening angle which is a multiple of $\alpha = \pi/n$ rad; thus $0 < \alpha < \pi/2$ for $n > 2$.

If n is not an integer, it is not possible to fill out a full neighbourhood of the conical stagnation point with these sectors, such that the velocity is continuous. Such flows may therefore only be obtained near a conical stagnation point on a body surface. Conical stagnation points away from a body surface can only occur if n is an integer. Sketches of the streamline patterns are given in figure 8 ($F_0 > 0$).

Substituting (16), (30) into (14) and using (7), we obtain for the pressure distribution, from (32),

$$\left(\frac{p}{p_0}\right)^{\gamma/(\gamma-1)} = 1 + \frac{2u_0(n-1)a_n}{1-u_0^2}\rho^n\cos n\phi + O(\rho^m) + O(\rho^{2n-2}). \tag{72}$$

The isobar pattern resulting from (72) shows a saddle character and is also sketched in figure 8. Comparison with the incompressible plane stagnation-point solution, which is a saddle-point-type flow in a corner with opening angle less than $\frac{1}{2}\pi$ rad, shows that the dominance of F_0 makes such a flow impossible in conical stagnation-point flows. It should be stressed, however, that this result is obtained under the assumption of potential flow and need not be valid in flows with entropy gradients. In fact, preliminary calculations show that such corner flows with entropy gradients exist. They may probably be used, in conjunction with oblique saddle-point flows, to describe the flow structure near flow separation from a body surface such as the flow past a circular cone at high angles of incidence. This structure was investigated by Fletcher (1975),

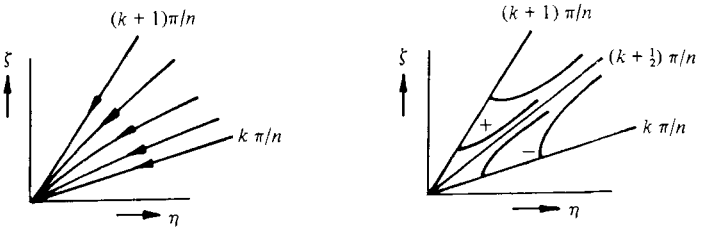

FIGURE 8. Starlike node ($n > 2$); (a) conical streamlines; (b) isobars.

Bannink & Nebbeling (1978), McRae & Hussaini (1978) and Nebbeling & Bannink (1978).

An example of the singularity for $n > 2$ is the conical stagnation point in a parallel flow (then $a_n = 0$). The isobars in figure 8 (b) do not apply in this case since the pressure is constant throughout the flow field.

4. Discussion

In order to illustrate the use of the classification of flows near conical stagnation points we discuss two flow problems: the supersonic flow past a symmetric external axial corner, and the flow past a circular cone at incidence.

An external corner may be formed by two intersecting wedges. In the symmetric case, where both wedge angles are equal and the leading-edge sweep of the wedges is the same, experiments and numerical calculations indicate that the conical flow pattern may be as sketched in figure 9 (a).

An oblique saddle point as discussed in § 3.1 may be observed in the corner point S. The nodal conical stagnation points N_1 and N_2 belong to the class treated in § 3.2 (figure 3, $0 < |\lambda| < \frac{1}{2}$).

The external corner flow was examined numerically by Kutler & Shankar (1976), Kutler, Pulliam & Vigneron (1979), and by Salas (1979). A local analysis near the corner point was given by Salas & Daywitt (1978) on the basis of the assumption that the velocity and the pressure gradient at the corner point are regular. However, if the including angle of the separatrices of an oblique saddle point lies between $\frac{2}{3}\pi$ and π radians, the solutions in the present investigation (equation (37)) have a singular pressure gradient at the corner point, which is also indicated by the numerical results of Kutler *et al.* (1979) and Salas (1979). In figure 9 (b) the results of the latter have been compared with an experimental pressure distribution obtained by the present authors on one face of a symmetric corner at conditions indicated in the figure. Both pressure distributions reveal clearly a minimum at the conical stagnation point N_1, which, according to § 3.2.1, figure 3, is characteristic for a nodal singularity with an infinite number of streamlines tangent to the body surface. The slight discrepancy between the experimental and theoretical data can mainly be explained by the small differences in flow conditions between the two cases.

In the inviscid supersonic flow past a circular cone at incidence several conical stagnation points may be observed. For a range of positive angles of incidence, with the exception of the lift-off angle, conical flow patterns are sketched in figure 10;

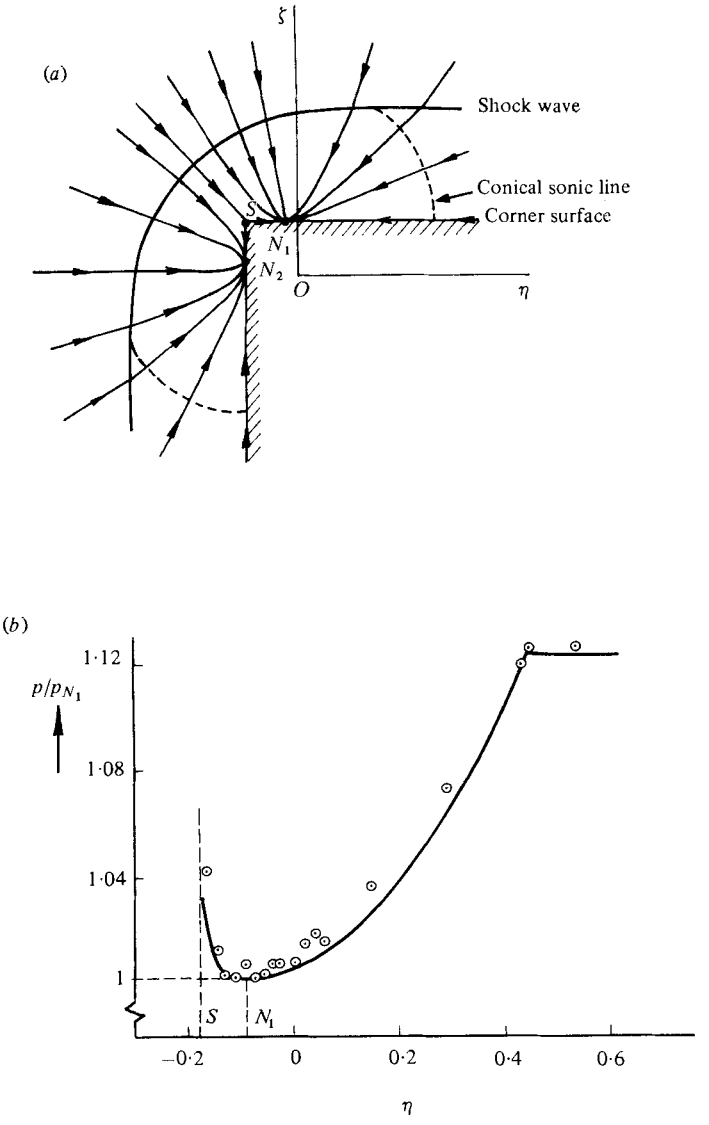

FIGURE 9. Conical flow past a symmetric external axial corner consisting of two intersecting wedges. (*a*) Conical streamlines with nodes N_1, N_2 and saddle point S. (*b*) Pressure distribution along surface. ⊙, experiment, free-stream Mach number, $M_\infty = 2{\cdot}95$, wedge angle of corner surface $\delta = 10{\cdot}3°$, leading-edge sweep $\Lambda = 0$; ——, numerical results of Salas (1979), $M_\infty = 3$, $\delta = 10°, \Lambda = 0$.

they contain saddle points and nodes which belong to the class $n = 2$, $|\lambda| \neq \frac{1}{2}$ (§ 3.2.1). These nodes and saddle points are well known from the literature on conical flow; in fact they already appear in one of the first papers on this subject (Ferri 1951). Particular attention has been given to the conical stagnation points in the leeward symmetry plane of the flow field. The change with incidence of the nodal character of this point on the body surface is discussed in several references, viz. Melnik (1967), Smith (1972), Bakker & Bannink (1974) and Bakker (1977).

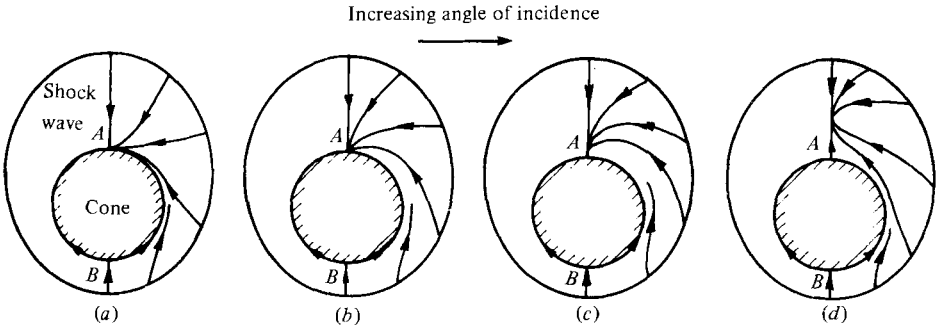

FIGURE 10. Inviscid conical flow past a circular cone at incidence; in A: (*a*) node tangential to cone surface, (*b*) starlike node, (*c*) node normal to cone surface, (*d*) saddle point (lift-off).

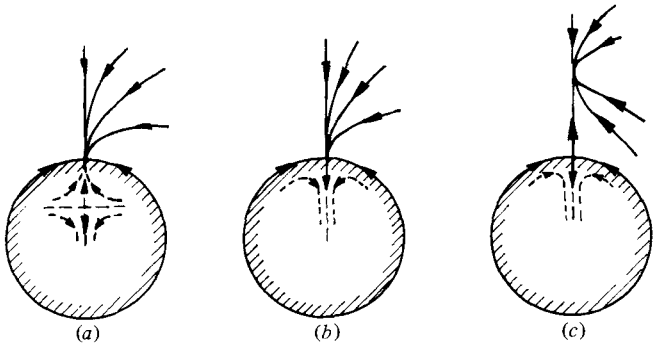

FIGURE 11. Inviscid conical flow past a circular cone at incidences near lift-off of singularity in A; incidence: (*a*) smaller than at lift-off, (*b*) at lift-off, (*c*) larger than at lift-off.

At high incidences lift-off of the singularity occurs (figure 10*d*), as already suggested by Ferri (1951). The lift-off phenomenon requires attention to the singularities found for $|\lambda| = \frac{1}{2}$ treated in § 3.2.2, and may then be viewed as a bifurcation phenomenon; this process is represented in figure 11.

At the lift-off angle of incidence, the conical stagnation point at the body surface in the leeward symmetry plane would be a saddle-node. The nodal part would be formed by the streamlines outside the body surface. The saddle part would be found if the flow around the body is extended inside the body.

Increasing the incidence beyond the lift-off angle makes the saddle-node fall apart into a saddle point attached to the cone surface and a node moving away from the body. Decreasing the angle of incidence below the lift-off angle would leave a nodal point on the cone surface and create a saddle point in the solution extended inside the cone. The calculations made by Bakker & Bannink (1974) to investigate conical stagnation points within the framework of slender-body theory may be used to support the conjecture that lift-off is a bifurcation phenomenon.

In experiments viscosity tends to obscure the lift-off phenomenon, which starts at the body surface where boundary-layer effects are dominant. In the experiments reported by Nebbeling & Bannink (1978) and (in an extension) by Bannink & Nebbeling (1978) it was shown that in the supersonic flow past slender cones at high incidences flow separation leads to the generation of a vortex system on the leeward

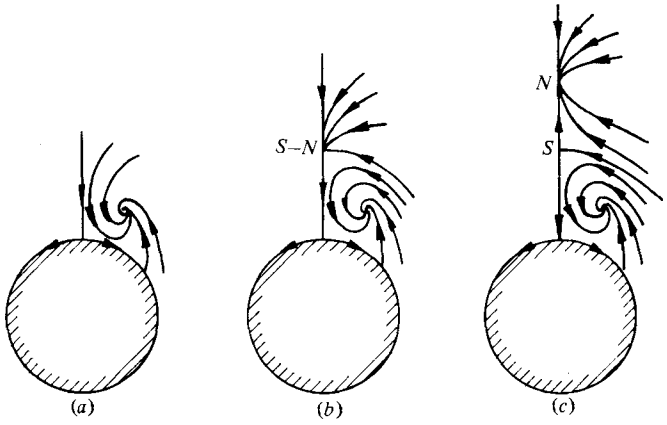

FIGURE 12. Conical flow past a circular cone at incidence, experimental observations. Bifurcation of a saddle-node (S–N) into a saddle (S) and a node (N); incidence: (a) smaller than at bifurcation, (b) at bifurcation, (c) larger than at bifurcation.

side of the cone. When increasing the angle of incidence of a cone, with a semi-apex angle of 7·5° in a supersonic flow with Mach number 2·94, from 17° to 22° another bifurcation phenomenon may be used to explain the appearance of a dividing streamline in the flow. This development has been depicted in figure 12, where the subsequent stages are shown at increasing angles of incidence.

According to Andronov *et al.* (1971) there are two ways in which a saddle-node may bifurcate. The first possibility is its falling apart into two structurally stable singularities and the other is its disappearance leaving no singularity at all.

The existence of the dividing streamline and the related saddle point in the leeward symmetry plane, accompanied by a nodal conical stagnation point higher above the cone surface (figure 12c), as was observed in the experiments by Bannink & Nebbeling (1978), may then be understood as a bifurcation from a saddle-node singularity (figure 12b) appearing at some angle of incidence between 17° and 22°. Below this angle of incidence the saddle-node of figure 12(b) has disappeared (figure 12a) and a conical flow field without a dividing streamline occurs.

REFERENCES

ANDRONOV, A. A., LEONTOVICH, E. A., GORDON, J. J. & MAIER, A. G. 1971 *Theory of Bifurcations of Dynamic Systems on a Plane*. Wiley.

ANDRONOV, A. A., LEONTOVICH, E. A., GORDON, J. J. & MAIER, A. G. 1973 *Qualitative Theory of Second-Order Dynamic Systems*. Wiley.

BAKKER, P. G. 1977 Conical streamlines and pressure distribution in the vicinity of conical stagnation points in isentropic flow. *Delft Univ. Technology, Dept Aerospace Engng, Rep.* LR-244.

BAKKER, P. G. & BANNINK, W. J. 1974 Conical stagnation points in the supersonic flow around slender circular cones at incidence. *Delft Univ. Technology, Dept Aerospace Engng, Rep.* VTH-184.

BANNINK, W. J. & NEBBELING, C. 1978 Measurements of the supersonic flow field past a slender cone at high angles of attack. *AGARD Conf. Proc.* 247, paper 22.

CODDINGTON, E. A. & LEVINSON, N. 1955 *Theory of Ordinary Differential Equations*. McGraw-Hill.

FERRI, A. 1951 Supersonic flow around circular cones at angles of attack. *N.A.C.A.* TR 1045.

FLETCHER, C. A. J. 1975 GTT method applied to cones at large angles of attack. *Proc. 4th Int. Conf. Numerical Methods in Fluid Dynamics* (ed. R. Richtmyer), Lecture Notes in Physics, vol. 35. Springer.

KUTLER, P., PULLIAM, T. H. & VIGNERON, Y. C. 1979 Computation of the viscous supersonic flow over external axial corners. *A.I.A.A. J.* **17**, 571–578.

KUTLER, P. & SHANKAR, V. 1976 Computation of the inviscid supersonic flow over an external axial corner. *Proc.* 1976 *Heat Transfer & Fluid Mech. Inst., Davis, Calif.*, pp. 356–373.

MCRAE, D. C. & HUSSAINI, M. Y. 1978 Numerical simulation of supersonic cone flow at high angle of attack. *AGARD Conf. Proc.* 247, paper 23.

MELNIK, R. E. 1967 Vortical singularities in conical flow. *A.I.A.A. J.* **5**, 631–637.

NEBBELING, C. & BANNINK, W. J. 1978 Experimental investigation of the supersonic flow past a slender cone at high incidence. *J. Fluid Mech.* **87**, 475–496.

SALAS, M. D. 1979 A careful numerical study of flowfields about external conical corners: Part 1. Symmetric configurations. *A.I.A.A. Paper* 79–1511.

SALAS, M. D. & DAYWITT, J. 1978 Structure of the flow field about external axial corners. *A.I.A.A. Paper* 78–59.

SMITH, J. H. B. 1972 Remarks on the structure of conical flow. In *Progress in Aerospace Sciences*, vol. 12, pp. 241–272. Pergamon.